

## Generating Isolated Elliptically Polarized Attosecond Pulses Using Bichromatic Counterrotating Circularly Polarized Laser Fields

Lukas Medišauskas\*

*Department of Physics, Imperial College London, South Kensington Campus, SW7 2AZ London, United Kingdom  
and Max-Born-Institute, Max-Born Strasse 2A, D-12489 Berlin, Germany*

Jack Wragg and Hugo van der Hart

*Centre for Theoretical Atomic, Molecular and Optical Physics, School of Mathematics and Physics,  
Queens University Belfast, Belfast BT7 1NN, United Kingdom*

Misha Yu. Ivanov

*Max-Born-Institute, Max-Born Strasse 2A, D-12489 Berlin, Germany  
Department of Physics, Humboldt University, Newtonstrasse 15, D-12489 Berlin, Germany  
and Department of Physics, Imperial College London, South Kensington Campus, SW7 2AZ London, United Kingdom*

(Received 29 April 2015; published 7 October 2015)

We theoretically demonstrate the possibility to generate both trains and isolated attosecond pulses with high ellipticity in a practical experimental setup. The scheme uses circularly polarized, counterrotating two-color driving pulses carried at the fundamental and its second harmonic. Using a model Ne atom, we numerically show that highly elliptic attosecond pulses are generated already at the single-atom level. Isolated pulses are produced by using few-cycle drivers with controlled time delay between them.

DOI: 10.1103/PhysRevLett.115.153001

PACS numbers: 32.80.Wr, 42.50.Tx, 42.65.Ky, 42.65.Re

High harmonic generation (HHG) in atoms and molecules is a highly nonlinear process that up-converts intense infrared laser field into the extreme ultraviolet (XUV) and soft x-ray radiation [1–4]. The emitted light can be used to track quantum dynamics underlying the nonlinear response [5–8], or as a tabletop source of bright, coherent, ultrashort pulses [9–12].

In the latter case, generation of circular or highly elliptic high harmonics and/or attosecond XUV pulses is very important. Such pulses would find numerous applications, e.g., in chiral-sensitive light-matter interactions such as chiral recognition via photoelectron circular dichroism [13–15], study of ultrafast chiral-specific dynamics in molecules [16,17], and x-ray magnetic circular dichroism spectroscopy [18–24], including time-resolved imaging of magnetic structures [18–22]. Tabletop sources of sub-100 fs, or even attosecond, chiral pulses would be a real breakthrough for laboratory-scale ultrafast studies. Not surprisingly, the search for schemes enabling the generation of short, coherent XUV pulses with tunable polarization is a very active area of research; see, e.g., Refs. [16,25–39].

Importantly, the control over polarization is desired not only for individual harmonics, where it has just been demonstrated [35,36], but also for individual attosecond pulses, both isolated and in a train, where a robust and practical scheme is still lacking. We show a way to solve this problem, proposing a practical scheme for the generation of highly elliptic attosecond pulses, both single and in a train.

An elegant solution to generating individual high harmonics with circular polarization has been found by Becker and

co-workers [28,29,31,32]; see also [40] for strongly related ideas. It relies on combining a circularly polarized fundamental field with a counterrotating second harmonic. The resulting electric field peaks three times within one cycle of the fundamental, producing three ionization bursts. The electron promoted to the continuum near the peak of the instantaneous field can successfully revisit the parent ion within about a half-cycle, emitting an attosecond radiation burst [28,29].

This approach has now been very successfully used in Refs. [35,36], demonstrating generation of bright, phase-matched high harmonic radiation. Importantly, tuning the ellipticity of one of the fields allows one to tune the ellipticity of the generated harmonics from linear to circular [35]. While the theoretical interpretation of this control is an interesting question in its own right [33,35], the approach is very promising. However, until now the possibility of extending this scheme from controlling the polarization of individual harmonics to controlling the polarization of isolated attosecond pulses looked far from straightforward.

Indeed, the driving field dictates that the direction of electron return rotates by  $120^\circ$  three times per cycle. Consequently, recombination with an  $s$  state yields three *linearly* polarized attosecond bursts per cycle, with polarization rotating by  $120^\circ$  from burst to burst [29].

This can also be seen in the frequency domain. The harmonic lines are at energies  $(n+1)\omega + 2n\omega = (3n+1)\omega$  and  $n\omega + (n+1)2\omega = (3n+2)\omega$ . In a centrally symmetric medium, and for circularly polarized driving fields, the selection rules dictate that the  $\Omega = (3n+1)\omega$  line

has the same helicity as the fundamental while the  $\Omega = (3n + 2)\omega$  line has the same helicity as the second harmonic ( $\Omega = n\omega + 2n\omega = 3n\omega$  is parity forbidden) [31,32,35,36,41,42]. Thus, the harmonics have alternating helicity. Adding harmonics of alternating helicity with equal intensity yields an attosecond pulse train where each subsequent pulse has linear polarization rotated by  $120^\circ$ , in concert with the time domain picture.

Suppressing every second allowed harmonic line, e.g.,  $\Omega^{(3n+2)} = (3n + 2)\omega$ , would solve the problem of generating individual attosecond pulses with circular polarization. Kfir *et al.* [36] suggested that such suppression can be achieved by optimizing the phase-matching conditions in a gas-filled hollow fiber and reported substantial suppression of the lines,  $\Omega^{(3n+2)} = (3n + 2)\omega$ .

Here, we show that relative intensities of the counterrotating harmonic lines strongly depend on the orbital momentum of the initial state. For an initial  $p$  state (as for neon, argon, or krypton gas), the harmonics corotating with the fundamental field can be much stronger than those corotating with the second harmonic. The effect is found with the contribution of both degenerate sublevels,  $p_+$  and  $p_-$ , included in the calculation. As a result, circularly polarized attosecond pulses are generated already at the microscopic, single-atom level; see Fig. 1. Additional help from phase matching is a bonus, but not necessary.

Next, we extend the scheme to generation of isolated attosecond pulses. We show that when the counterrotating driving pulses become relatively short, e.g., 7–8 fs for the 800 nm driver and its second harmonic, one can generate an isolated attosecond pulse, or a controllable train with 2 or 3 pulses, by tuning the time delay between the fundamental and the second harmonic.

To demonstrate these effects, we numerically solve the time-dependent Schrödinger equation (TDSE) for a 2D neonlike model atom, for counterclockwise (+) polarized fundamental and clockwise (−) polarized second harmonic. We show that the harmonics generated from orbitals with  $m = \pm 1$  differ from those generated from  $s$  orbitals in two important ways. Firstly, the height of the adjacent left- and right-circularly polarized harmonics can differ by an order of magnitude, with the  $m = 1$  state favoring harmonics corotating with the fundamental and the  $m = -1$  state favoring harmonics corotating with the  $2\omega$  field. Secondly, once the two contributions are added coherently, + polarization continues to dominate in a broad spectral range, leading to a highly elliptic circularly polarized attosecond pulse train already at the single-atom level. Our findings are in accord with Ref. [36] (see Ne spectra in Fig. 3 of Ref. [36]), where such disparity was attributed to phase matching.

We solve the TDSE in the length gauge (atomic units are used throughout unless stated otherwise):

$$i\frac{\partial}{\partial t}\Phi(t, r) = [\hat{T} + V(r) + \mathbf{r} \cdot \mathbf{E}(t)]\Phi(t, r). \quad (1)$$

The 2D model potential is taken from [43]:

$$V(r) = -\frac{Z(r)}{\sqrt{r^2 + a}}, \quad (2)$$

where  $Z(r) = 1 + 9\exp(-r^2)$  and  $a = 2.88172$  to obtain the ionization potential of the Ne atom  $I_p = 0.793$  a.u. for the  $2p$  orbitals. The  $1s$  state has an energy  $E_{1s} = -2.952$  a.u. and the  $2s$  energy is  $E_{2s} = -0.217$  a.u.. For reference calculations we use  $1s$  as the initial state but keep the same ionization potential taking  $Z(r) = 1$  and  $a = 0.1195$ . The laser electric field is

$$E(t) = E_{ir}f(t)(\cos[\omega t] + \cos[2\omega t])\hat{x} + E_{ir}f(t)(\sin[\omega t] - \sin[2\omega t])\hat{y}, \quad (3)$$

where  $f(t)$  is the trapezoidal envelope with 2 cycle rising and falling edges and 5 cycle plateau (in units of fundamental). The  $\omega$  field rotates counterclockwise (+). The second harmonic rotates clockwise (−).

The TDSE is propagated on a 2D Cartesian grid using a Taylor-series propagator with expansion up to eighth order [44]. A complex absorbing potential,

$$V_c(x) = \eta(x - x_0)^n, \quad (4)$$

with  $\eta = 5 \times 10^{-4}$  and  $n = 3$  is used to avoid nonphysical reflections from the boundary. Other simulation parameters are summarized in Table I.

Convergence was tested with respect to the absorbing potential, the time step, and the spatial grid. Note that HHG in bicircular fields is dominated by very short trajectories [28].

The initial wave functions were obtained using imaginary time propagation filtering out the ground state wave function to obtain  $p_x$  and  $p_y$  orbitals. The  $p_\pm$  states are defined as  $p_\pm = p_x \pm ip_y$ . The laser intensity was kept such as not to exceed 5% ionization and to avoid strong shifts and mixing of the degenerate atomic orbitals described in Ref. [43]. The spectra were obtained by performing the Fourier transform of the time-dependent dipole acceleration, evaluated at every 0.5 a.u.

The results are robust with the variation of the pulse length, the shape and length of its rising and falling edges, laser intensity, and wavelength: we performed calculations from  $\lambda = 600$  nm up to  $\lambda = 1200$  nm.

Figure 1(a) shows reference spectra obtained for the  $1s$  initial state of the model potential with  $I_p$  of neon. It agrees well with previously published results [28,32,35,36]; the harmonics come in pairs  $(n + 1)\omega + n2\omega = (3n + 1)\omega$

TABLE I. Parameters of the calculations in atomic units unless stated otherwise.

Laser frequency	$\omega$	0.05	( $\lambda = 911$ nm)
Laser electric field	$E_{ir}$	0.05	( $I = 0.88 \times 10^{14}$ W/cm <sup>2</sup> )
Grid step size	$dr$	0.2	
Time step size	$dt$	0.005	
Propagation time	$T$	1250	(30.2 fs)
Maximal grid extent	$X_{\max}$	$\pm 60$	
Absorbing boundary	$x_0$	$\pm 36$	

and  $n\omega + (n+1)2\omega = (3n+2)\omega$  of similar heights. The left harmonic in the pair has the same polarization as the fundamental field; the right harmonic follows the  $2\omega$  driver. The harmonics  $3n\omega$  are parity forbidden.

Figures 1(b) and 1(c) show spectra for the  $p_+$  and  $p_-$  initial states. For the  $p_+$  initial state, the harmonics that have the same polarization as the driving IR field are preferred. For the  $p_-$  initial state, the harmonics with the same polarization as the  $2\omega$  driver are stronger. There are additional spectral variations in the plateau region, different for  $p_+$  and  $p_-$  orbitals. There is also a qualitative difference between the below-threshold ( $<I_p$ ) and above-threshold ( $>I_p$ ) harmonics, showing that the evolution of the

photoelectron in the continuum is critical for the observed propensity in the harmonic strengths.

Figure 1(d) shows the spectra obtained from adding the contributions from the  $p_+$  and  $p_-$  orbitals coherently, as required. In the plateau region, harmonics with the same polarization as the driving IR field dominate over those with opposite polarization.

The subcycle dynamics of the emission process was analyzed using the Gabor transform (GT) [45] of the time-dependent acceleration dipoles  $a(t)$ :

$$\text{GT}[\Omega, t_0] = \frac{1}{2\pi} \int dt a(t) e^{-i\Omega t} e^{-(t-t_0)^2/(2T^2)}, \quad (5)$$

where we have chosen  $T = 1/3\omega$ . The reference spectrograms for the  $1s$  initial state in Figs. 2(a) and 2(b) show the time-dependent intensity [2(a)] and ellipticity [2(b)] for time-resolved spectra, in the regions where spectral amplitudes are significant. As expected, there are three radiation bursts per  $\omega$  cycle with linear polarization, as predicted in Refs. [28,29,32].

Figures 2(c) and 2(d) show the same spectrogram for the  $2p$  state, i.e., the coherent superposition of the radiation from  $p_+$  and  $p_-$  states. Although the signal strength in the spectrogram is similar to the  $s$  orbital, the ellipticity of the emitted radiation is very different. Three distinct regions can be identified: (i) below threshold region, where the ellipticity is mostly negative, (ii) the middle region, where the ellipticity is high and positive, and (iii) near cutoff region where the emitted radiation is mostly linear. The energy region (ii) of the spectrogram coincides with the spectral window in Fig. 1(d) where the difference between clockwise and counterclockwise harmonics is the greatest.

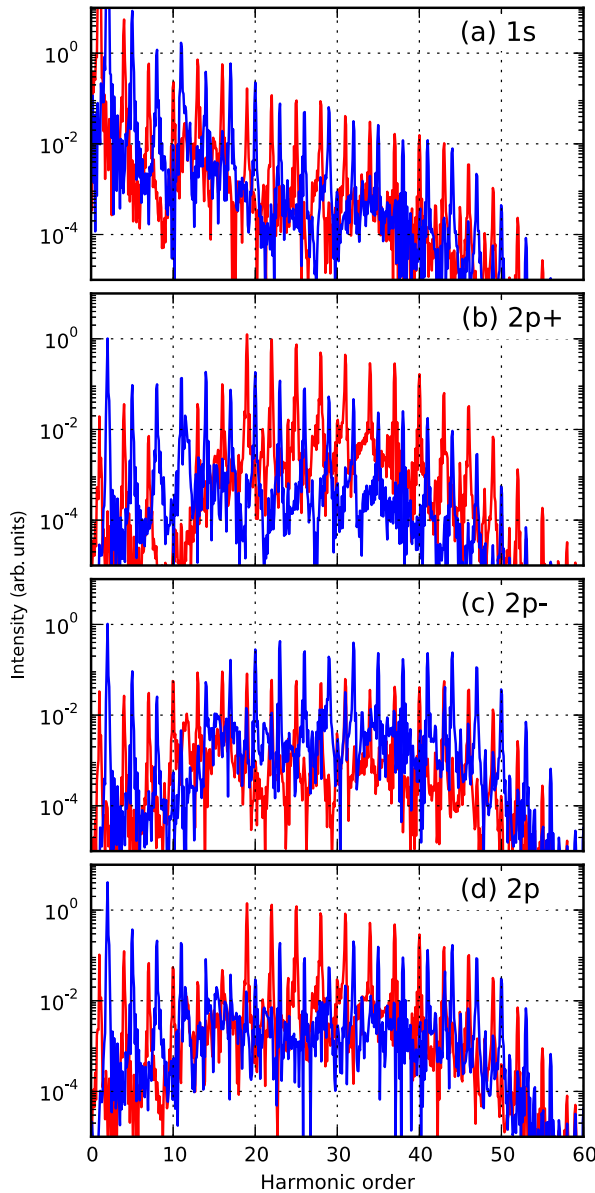


FIG. 1 (color online). Spectra for (a)  $1s$ , (b)  $2p_+$ , (c)  $2p_-$  initial states, and (d) equal mixture of  $2p_+$  and  $2p_-$  states. Colors mark harmonics corotating (red) and counterrotating (blue) with the  $\omega$  field.

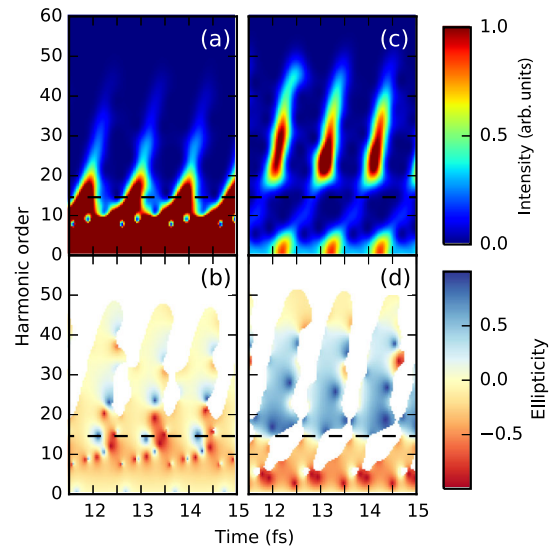


FIG. 2 (color online). Time-resolved XUV emission intensity and ellipticity from (a),(b)  $1s$  and (c),(d)  $2p$  orbitals. Color in (b) and (d) indicates the ellipticity of the spectral components in the regions where the amplitude of the spectrogram is significant. The horizontal dashed lines mark the  $I_p$ .

Application of bicircular fields is naturally extended from the generation of an attosecond pulse train to the generation of an isolated attosecond pulse, using short driving pulses and changing the time delay between them. Indeed, the harmonic emission driven by circular fields is only possible when the two counterrotating circular pulses overlap. Given the high nonlinearity of the overall process (including ionization), it will be limited to the temporal window where the two driving pulses overlap with nearly equal and high intensity. This idea is tested in Fig. 3, which shows time-resolved spectrograms and ellipticity of the emitted light for  $\lambda = 800$  and  $400$  nm counterrotating drivers with full width at half maximum duration of  $4$  fs and  $\sin^2$  envelope with  $I = 1.7 \times 10^{14}$  W/cm<sup>2</sup> peak intensity, for two time delays. In the case of perfect overlap, three attosecond pulses are generated. Delaying the low-frequency pulse by  $2.6$  fs (full period of  $800$  nm field) yields two attosecond pulses with strong ellipticity, that are well separated in energy. An isolated pulse would be obtained by filtering the lower or higher energy pulse. With shorter driving pulses, a single isolated attosecond pulse will be generated.

What is the physical origin of the HHG sensitivity to the angular momentum of the initial state? The energy and angular momenta that the electron accumulates from the laser field while propagating in the continuum are transferred to the harmonic photon upon recombination. The matrix elements associated with recombination are the complex conjugate of the photoionization matrix elements. In 2D one photon ionization with the field corotating with the

initial state is much more likely than with counterrotating field. This is a direct analogue of Fano-Bethe propensity rules [46] and is also the case for Rydberg states corotating and counterrotating with the field [47,48].

Consider the harmonic spectra from the  $p_+$  orbital. The right-circularly polarized harmonics result from the  $(n+1)\omega + n2\omega$  pathway. The recombination step is conjugated to photoionization from the  $p_+$  state with a corotating field, favored by the propensity rules. The left-circularly polarized harmonics result from the  $n\omega + (n+1)2\omega$  pathway. The recombination step is conjugated to photoionization from the  $p_+$  state with a counterrotating field, disfavored by the propensity rules. This explains the relative heights of the harmonic pairs for the  $p_+$  initial state. The same analysis explains why harmonics corotating with the  $2\omega$  field are preferred for the  $p_-$  initial state.

But why is  $p_+$  dominant over  $p_-$ ? The answer lies in the stronger effect of the lower-frequency (counterclockwise) field on the continuum electron, which leads to higher population of the continuum states with positive angular momentum than the population with the negative angular momentum. The more probable recombination from such states is to the  $p_+$  state, by emitting light with counterclockwise polarization.

The carrier-envelope phase stabilization controls the orientation of the polarization ellipse of the attosecond pulse, but not the pulse. Indeed, as long as the relative phase between the two pulses,  $\omega$  and  $2\omega$ , is locked, changing the carrier-envelope phase will rotate the trefoil pattern of the driving field and thus the polarization ellipse of the attosecond pulse but will not alter its high ellipticity. This property, in combination with the possibility of using relatively routine durations of the two driving pulses, makes the scheme extremely attractive for practical implementation.

Finally, we comment on the difference between the 2D model presented here and a 3D system. Since the harmonic dipole for the  $m = 0$  orbital is negligible, the only expected difference is the additional spreading of the continuum electron wave packet in the direction perpendicular of the plane of polarization of the driving field. Such spreading is identical for both  $p_+$  and  $p_-$  orbitals and thus will not change the relative intensity of the corresponding harmonics. Consequently, we expect that our results stand in the full 3D case. In this context, we would also like to bring the reader's attention to the recent 3D strong field approximation calculations of HHG for a Ne atom in a two-color bicircular field [49] where similar results of the intensity of left- and right-circularly polarized harmonics from  $m = \pm 1$  orbitals have also been found.

We thank Emilio Pisanty, Felipe Morales, Wilhelm Becker, and Dejan Milošević for valuable discussions. Financial support from the FP7 Marie Curie ITN CORINF, the EPSRC Programme Grant No. EP/I032517/1, and partially from the U.S. Air Force Office of Scientific Research under program No. FA9550-12-1-0482 is acknowledged.

The computer codes and data used to produce this Letter can be downloaded from Ref. [50].

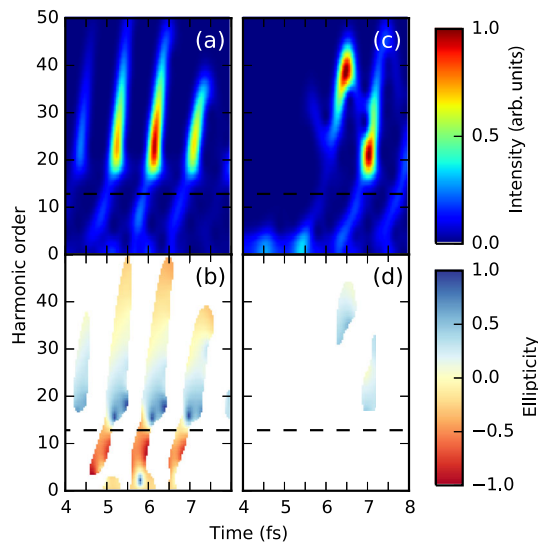


FIG. 3 (color online). Time-resolved XUV emission from a  $2p$  orbital, for time-delayed  $4$  fs full width at half maximum  $800$  and  $400$  nm pulses. (a) Spectral intensity and (b) time-dependent ellipticity for perfect overlap of the two pulses. (c) Spectral intensity and (d) time-dependent ellipticity for the two-pulse delay of  $2.6$  fs. Spectra in (c) is multiplied by a factor of  $2$  to enhance the contrast. Color in (b) and (d) indicates the ellipticity of the spectral components in the regions where the amplitude of the spectrogram is significant. The horizontal dashed lines mark the  $I_p$ .

- \*Corresponding author.  
lukas.medisauskas@imperial.ac.uk
- [1] P. Salières, A. L’Huillier, P. Antoine, and M. Lewenstein, *Study of the Spatial and Temporal Coherence of High-Order Harmonics* (Academic Press, New York, 1999) pp. 83–142.
- [2] F. Krausz and M. Ivanov, *Rev. Mod. Phys.* **81**, 163 (2009).
- [3] P. B. Corkum, *Phys. Rev. Lett.* **71**, 1994 (1993).
- [4] M. Lewenstein, P. Balcou, M. Y. Ivanov, A. L’Huillier, and P. B. Corkum, *Phys. Rev. A* **49**, 2117 (1994).
- [5] S. Haessler, J. Caillat, W. Boutu, C. Giovanetti-Teixeira, T. Ruchon, T. Auguste, Z. Diveki, P. Breger, A. Maquet, B. Carré, R. Taïeb, and P. Salières, *Nat. Phys.* **6**, 200 (2010).
- [6] S. Baker, J. Robinson, C. Haworth, H. Teng, R. A. Smith, C. C. Chirilă, M. Lein, J. W. G. Tisch, and J. P. Marangos, *Science* **312**, 424 (2006).
- [7] H. J. Wörner, J. B. Bertrand, D. V. Kartashov, P. B. Corkum, and D. M. Villeneuve, *Nature (London)* **466**, 604 (2010).
- [8] O. Smirnova, Y. Mairesse, S. Patchkovskii, N. Dudovich, D. Villeneuve, P. Corkum, and M. Y. Ivanov, *Nature (London)* **460**, 972 (2009).
- [9] A. L. Cavalieri, N. Müller, T. Uphues, V. S. Yakovlev, A. Baltuška, B. Horvath, B. Schmidt, L. Blümel, R. Holzwarth, S. Hendel, M. Drescher, U. Kleineberg, P. M. Echenique, R. Kienberger, F. Krausz, and U. Heinzmann, *Nature (London)* **449**, 1029 (2007).
- [10] T. Popmintchev, M. C. Chen, D. Popmintchev, A. Paul, S. Brown, S. Ališauskas, G. Andriukaitis, T. Balčinas, O. D. Mücke, A. Pugzlys, A. Baltuška, B. Shim, S. Schrauth, A. Gaeta, C. Hernández-García, L. Plaja, A. Becker, A. Jaron-Becker, M. M. Murnane, and H. C. Kapteyn, *Science* **336**, 1287 (2012).
- [11] P. Salières, L. LeDéroff, T. Auguste, P. Monot, P. d’Oliveira, D. Campo, J. F. Hergott, H. Merdji, and B. Carré, *Phys. Rev. Lett.* **83**, 5483 (1999).
- [12] F. Lépine, G. Sansone, and M. J. Vrakking, *Chem. Phys. Lett.* **578**, 1 (2013).
- [13] U. Hergenhahn, E. E. Rennie, O. Kugeler, S. Marburger, T. Lischke, I. Powis, and G. Garcia, *J. Chem. Phys.* **120**, 4553 (2004).
- [14] N. Böwering, T. Lischke, B. Schmidtke, N. Müller, T. Khalil, and U. Heinzmann, *Phys. Rev. Lett.* **86**, 1187 (2001).
- [15] I. Powis, *J. Chem. Phys.* **112**, 301 (2000).
- [16] A. Ferré, C. Handschin, M. Dumergue, F. Burgy, A. Comby, D. Descamps, B. Fabre, G. A. Garcia, R. Géneaux, L. Merceron, E. Mével, L. Nahon, S. Petit, B. Pons, D. Staedter, S. Weber, T. Ruchon, V. Blanchet, and Y. Mairesse, *Nat. Photonics* **9**, 93 (2014).
- [17] O. Travnikova, J.-C. Liu, A. Lindblad, C. Nicolas, J. Söderström, V. Kimberg, F. Gelbukhanov, and C. Miron, *Phys. Rev. Lett.* **105**, 233001 (2010).
- [18] I. Radu, K. Vahaplar, C. Stamm, T. Kachel, N. Pontius, H. A. Dürr, T. A. Ostler, J. Barker, R. F. L. Evans, R. W. Chantrell, A. Tsukamoto, A. Itoh, A. Kirilyuk, T. Rasing, and A. V. Kimel, *Nature (London)* **472**, 205 (2011).
- [19] C. Boeglin, E. Beaurepaire, V. Halté, V. López-Flores, C. Stamm, N. Pontius, H. A. Dürr, and J.-Y. Bigot, *Nature (London)* **465**, 458 (2010).
- [20] S. Eisebitt, J. Lüning, W. F. Schlotter, M. Lörger, O. Hellwig, W. Eberhardt, and J. Stöhr, *Nature (London)* **432**, 885 (2004).
- [21] P. Fischer, T. Eimüller, G. Schütz, G. Schmahl, P. Guttman, and G. Bayreuther, *J. Magn. Magn. Mater.* **198-199**, 624 (1999).
- [22] V. López-Flores, J. Arabski, C. Stamm, V. Halté, N. Pontius, E. Beaurepaire, and C. Boeglin, *Phys. Rev. B* **86**, 014424 (2012).
- [23] J. Stöhr, Y. Wu, B. D. Hermsmeier, M. G. Samant, G. R. Harp, S. Koranda, D. Dunham, and B. P. Tonner, *Science* **259**, 658 (1993).
- [24] G. Schütz, M. Knülle, and H. Ebert, *Phys. Scr.* **T49A**, 302 (1993).
- [25] F. Chen, J. Luo, and F. Luo, *Opt. Commun.* **342**, 68 (2015).
- [26] F. Morales, I. Barth, V. Serbinnenko, S. Patchkovskii, and O. Smirnova, *J. Mod. Opt.* **59**, 1303 (2012).
- [27] K.-J. Yuan and A. D. Bandrauk, *Phys. Rev. Lett.* **110**, 023003 (2013).
- [28] D. B. Milošević, W. Becker, and R. Kopold, *Phys. Rev. A* **61**, 063403 (2000).
- [29] D. B. Milošević and W. Becker, *Phys. Rev. A* **62**, 011403 (2000).
- [30] K.-J. Yuan and A. D. Bandrauk, *Phys. Rev. A* **84**, 023410 (2011).
- [31] H. Eichmann, A. Egbert, S. Nolte, C. Momma, B. Wellegehausen, W. Becker, S. Long, and J. K. McIver, *Phys. Rev. A* **51**, R3414 (1995).
- [32] S. Long, W. Becker, and J. K. McIver, *Phys. Rev. A* **52**, 2262 (1995).
- [33] E. Pisanty, S. Sukiasyan, and M. Ivanov, *Phys. Rev. A* **90**, 043829 (2014).
- [34] M. Ivanov and E. Pisanty, *Nat. Photonics* **8**, 501 (2014).
- [35] A. Fleischer, O. Kfir, T. Diskin, P. Sidorenko, and O. Cohen, *Nat. Photonics* **8**, 543 (2014).
- [36] O. Kfir, P. Grychtol, E. Turgut, R. Knut, D. Zusin, D. Popmintchev, T. Popmintchev, H. Nembach, J. M. Shaw, A. Fleischer, H. Kapteyn, M. Murnane, and O. Cohen, *Nat. Photonics* **9**, 99 (2014).
- [37] W. Becker, B. N. Chichkov, and B. Wellegehausen, *Phys. Rev. A* **60**, 1721 (1999).
- [38] K.-J. Yuan and A. D. Bandrauk, *J. Phys. B* **45**, 074001 (2012).
- [39] G. Lambert, B. Vodungbo, J. Gautier, B. Mahieu, V. Malka, S. Sebban, P. Zeitoun, J. Luning, J. Perron, A. Andreev, S. Stremoukhov, F. Ardana-Lamas, A. Dax, C. P. Hauri, A. Sardinha, and M. Fajardo, *Nat. Commun.* **6**, 6167 (2015).
- [40] T. Zuo and A. D. Bandrauk, *J. Nonlinear Opt. Phys. Mater.* **04**, 533 (1995).
- [41] O. E. Alon, V. Averbukh, and N. Moiseyev, *Phys. Rev. Lett.* **80**, 3743 (1998).
- [42] F. Mauger, A. D. Bandrauk, A. Kamor, T. Uzer, and C. Chandre, *J. Phys. B* **47**, 041001 (2014).
- [43] I. Barth and M. Lein, *J. Phys. B* **47**, 204016 (2014).
- [44] C. Moler and C. V. Loan, *SIAM Rev.* **20**, 801 (1978).
- [45] C. C. Chirilă, I. Dreisigacker, E. V. van der Zwan, and M. Lein, *Phys. Rev. A* **81**, 033412 (2010).
- [46] U. Fano, *Phys. Rev. A* **32**, 617 (1985).
- [47] K. Rzażewski and B. Piraux, *Phys. Rev. A* **47**, R1612 (1993).
- [48] J. Zakrzewski, D. Delande, J. C. Gay, and K. Rzażewski, *Phys. Rev. A* **47**, R2468 (1993).
- [49] D. Milošević, *Opt. Lett.* **40**, 2381 (2015).
- [50] <http://staff.mbi-berlin.de/medisaus>.